Catalysis Today 158 (2010) 220–227

Contents lists available at ScienceDirect

Catalysis Today

journal homepage: www.elsevier.com/locate/cattod

Au nanoparticles dispersed on functionalized mesoporous silica for selective oxidation of cyclohexane

Pingping Wu [a,b], Peng Bai [a], Kian Ping Loh [b,c], X.S. Zhao [a,b,*]

[a] *Department of Chemical and Biomolecular Engineering, National University of Singapore, 4 Engineering Drive, 117576 Singapore, Singapore*
[b] *Nanoscience and Nanotechnology Initiative, National University of Singapore, 117576 Singapore, Singapore*
[c] *Department of Chemistry, National University of Singapore, 3 Science Drive, 117543 Singapore, Singapore*

ARTICLE INFO

Article history:
Available online 24 April 2010

Keywords:
Gold nanoparticle
Functionalization
Mesoporous silica
Cyclohexane oxidation

ABSTRACT

A one-pot method was used to synthesize vinyl-functionalized mesoporous silica with highly dispersed gold nanoparticles. Samples were characterized using physical adsorption of nitrogen, X-ray diffraction, transmission electronic microscope, solid-state nuclear magnetic resonance, X-ray photoelectron spectrometer, and ultraviolet–visible spectrometer. It was found that Au was anchored on the vinyl functionality as highly dispersed and uniform nanoparticles. Catalytic results showed that such Au nanoparticles displayed very high catalytic activity and selectivity in solvent-free selective oxidation of cyclohexane with molecular oxygen.

1. Introduction

Selective oxidation of hydrocarbons by air/molecular oxygen, a significant process in the chemical industry, provides a greener route for the synthesis of fine chemicals and intermediates. Selective oxidation of cyclohexane is such a reaction. Its products, cyclohexanol and cyclohexanone (also known as K/A oil), are important chemical intermediates for the bulk production of polyamide and plastics, such as Nylon 6 and Nylon 6, 6. Transition metal salts such as Mn and Co naphthenates are the main catalysts currently used in the industry. The use of such homogeneous catalysts is undesirable in these environmentally conscious and energy-intensive days.

Solid catalysts, such as titanium silicalite-1 (TS-1) [1,2], metal-substituted aluminophosphate molecular sieves (MAlPOs, where M stands for Cr, Co, Fe, Ce, Cu, and Mn, etc.) [3–5], and metal-incorporated mesoporous and microporous aluminosilicates molecular sieves (M-MCM-41, M-MCM-48, M-ZSM-5) [6–8], have been explored as heterogeneous catalysts for cyclohexane oxidation. These catalysts in general exhibit a relatively low activity and/or selectivity. On the other hand, nanostructured catalysts, such as Fe_2O_3, Co_3O_4, and mixed Fe–Co oxide nanoparticles [9–11] have been examined in the cyclohexane oxidation as well. These catalyst systems suffer from a poor mechanical stability [12].

Since gold (Au) was found to display a surprisingly high catalytic activity in the oxidation of CO at low temperatures [13–16], numerous investigations have been carried out to explore its use as a catalyst in various industrially important processes. Au nanoparticles supported on porous solids, such as Au/ZSM-5 [17], Au/MCM-41 [18,19] and Au/Al_2O_3 catalysts [20,21], have been studied in the cyclohexane oxidation to produce cyclohexanol and cyclohexanone. It was observed that for the one-pot hydrothermal synthesized Au/ZSM-5 and Au/MCM-41 catalysts, aggregation of Au nanoparticles to form larger ones occurred during high-temperature calcination for removing the template and the serious leaching of Au particles during the reaction is also problematic [4]. The aggregation and leaching of Au nanoparticles resulted in a low activity for cyclohexane oxidation and poor stability of Au catalyst.

Mesoporous SBA-15 [22] has proven to be a better catalyst support for Au catalyst in comparison with other mesoporous silica materials, including HMS, MCM-41, MCM-48, SBA-16, because of its two-dimensional (2D) hexagonal pore structure, large pore size and strong pore wall to immobilize the particles trapped inside the pores [23,24]. It was also been found that [25] Au nanoparticles are mobile on silica surface due to weak interactions between the Au nanoparticles and the support. In order to firmly anchor Au nanoparticles on the silica surface, stabilizing ligands have been used to modify the mesoporous silica. Zhu et al. modified SBA-15 with amine and thiol groups for preparing Au/SBA-15 catalysts [26]. The authors observed that Au particle supported on the functionalized SBA-15 support exhibited higher activity and selectivity in cyclohexane oxidation than that supported on unmodified SBA-15 silica.

In this work, Au nanoparticles supported on functionalized mesoporous silicas were prepared using a one-pot method, in

* Corresponding author at: Department of Chemical and Biomolecular Engineering, National University of Singapore, 4 Engineering Drive, Singapore 117576, Singapore. Tel.: +65 65164727; fax: +65 67791936.
E-mail address: chezxs@nus.edu.sg (X.S. Zhao).

0920-5861/$ – see front matter © 2010 Elsevier B.V. All rights reserved.
doi:10.1016/j.cattod.2010.03.027

which vinyl functionality was used as functional ligands to stabilize Au nanoparticles. By co-condensation of tetraethyl orthosilicate (TEOS) and vinyl triethoxysilane (VTES) in the presence of Au precursor, Au nanoparticles were anchored on the organically functionalized SBA-15 support in a highly dispersed and uniform manner. The catalytic results showed that the catalyst displayed a very high activity and selectivity in solvent-free selective oxidation of cyclohexane using molecular oxygen.

2. Experimental

2.1. Chemicals

$HAuCl_4 \cdot xH_2O$ (Aldrich), tetraethyl orthosilicate (TEOS, 98%, Acros Organics), triblock copolymer P123 (Aldrich), vinyl triethoxysilane (VTES, 97%, Aldrich), hydrochloric acid (37%, Merck), absolute ethanol (99.98%, Merck) were used as received without further purification.

2.2. Preparations of catalysts

For the one-pot synthesis, 4 g of P123 was dissolved in 30 mL of deionized water at room temperature followed by adding 120 mL of a 0.74 M HCl solution. 0.38 g VTES and 8.4 g TEOS with a molar ratio of VTES:TEOS = 1:20 were slowly added. 6.4 mL of 0.02 M $HAuCl_4 \cdot xH_2O$ solution (for a Au loading of 1 wt%) was introduced into the synthesis system. After stirring at 40 °C for 24 h, the mixture was transferred to a Teflon-lined stainless steel autoclave to undergo a static hydrothermal treatment at 100 °C for 24 h. The solids were filtered off, washed with deionized water till no Cl^- was detected using a $AgNO_3$ solution, and dried at 100 °C overnight. Template removal was conducted using the ethanol extraction method at 70 °C for 6 h. This process was repeated three times. The Au catalysts thus synthesized is designated as Au/F-SBA-15-co.

For comparison purposes, Au nanoparticles supported on an non-functionalized SBA-15 silica (denoted as Au/SBA-15-co) was also synthesized using the same synthesis protocol except that no organosilane was added and the template was removed by calcination at 550 °C for 8 h. Catalyst Au/F-SBA-15-co was reduced in a H_2 flow at 250 °C for 2 h with a heating rate of 5 °C/min, while catalyst Au/SBA-15-co was auto-reduced during calcination.

The impregnation method was also used to prepare another two Au catalysts supported on SBA-15 and organically functionalized SBA-15. The samples thus prepared are designated as Au/SBA-15-im and Au/F-SBA-15-im, respectively. 1 g of SBA-15 or F-SBA-15 was dispersed in 2.52 mL of 0.02 M chloroauric acid tetrahydrate ($HAuCl_4 \cdot 4H_2O$) solution and 17.5 mL of deionized water. The slurry was stirred for 2 h at room temperature, followed by sonication for 20 min. The resulting product was evaporated to less than 2 mL and dried in an oven at 60 °C for 48 h, and finally reduced in a flowing H_2 at 250 °C for 2 h at a heating rate of 5 °C/min.

2.3. Characterization

X-ray powder diffraction (XRD) patterns were recorded on a XRD-6000 (Shimadzu, Japan) system with a Cu Kα radiation of wavelength $\lambda = 0.15418$ nm. N_2 adsorption–desorption isotherms were measured at −196 °C on an automatic volumetric sorption analyzer (Quantachrome, NOVA1200). Prior to adsorption, the samples were degassed at 300 °C for 3 h under vacuum. Ultraviolet–visible (UV–vis) spectra were measured on a UV–vis–NIR scanning spectrophotometer (Shimudzu, UV-3101 PC) with an ISR-3100 integrating sphere attachment and $BaSO_4$ as an internal reference. X-ray photoelectron spectroscopy (XPS) spectra were recorded on an AXIS HIS 165 spectrometer (Kratos Analytical) with a monochromatized Al Ka X-ray source. The Au 4f signals were recorded in a 0.05 eV step with a pass energy of 40 eV. Solid-state ^{13}C cross-polarization (CP) with ^1H magic-angle spinning (MAS) nuclear magnetic resonance (NMR) spectra were collected on a Bruker DRX400 FT-NMR spectrometer. The microscopic features of the catalysts were observed on a transmission electron microscope (JEM 2010 from JEOL) operated at 200 kV.

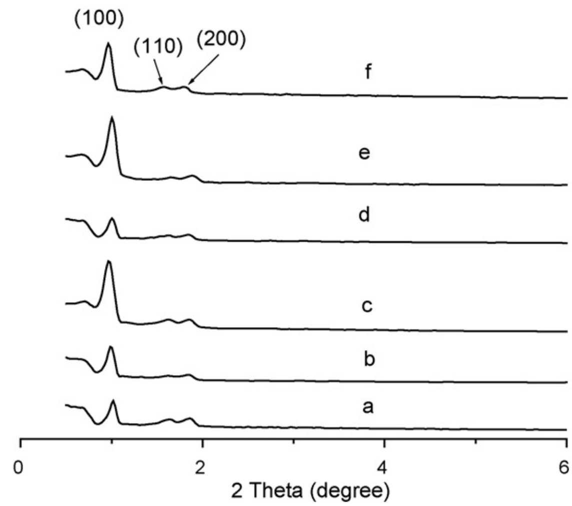

Fig. 1. Low-angle X-ray diffraction patterns of (a) SBA-15; (b) F-SBA-15; (c) Au/SBA-15-im; (d) Au/F-SBA-15-im; (e) Au/SBA-15-co and (f) Au/F-SBA-15-co.

2.4. The selective oxidation of cyclohexane by molecular oxygen

The selective oxidation of cyclohexane was carried out in a 200 mL Parr batch reactor with a polytetrafluoroethylene (PTFE) liner. 20 mL of cyclohexane and 50 mg solid catalyst were added into the reactor. After purging with O_2, the reactor was heated to 150 °C and the O_2 pressure was adjusted to 1 MPa. During the oxidation process, the O_2 pressure was kept between 0.8 and 1 MPa with a stirring rate of 300 rpm. After 2 h of reaction, the reactor was cooled down to 30 °C and the mixture was mixed with ethanol. An excessive amount of triphenylphosphine was added to the reaction mixture to completely reduce cyclohexyl hydroperoxide (CHHP) which is an intermediate in reaction. The products were analyzed using a gas chromatogram (HP 6890 series GC) with a mass spectrometer detector (HP 5973 mass selective detector) and a capillary column (HP 5MS).

3. Results and discussion

3.1. Characterization of the catalysts

Fig. 1 shows the low-angle XRD patterns of the samples prepared in this work. It is seen that all samples exhibited one strong and two weak diffraction peaks, characteristic of a two-dimensional (2D) hexagonal mesostructure with a *p6mm* space group, indicating these samples are well-ordered mesostructures. The strong (1 0 0) diffraction peak together with the appearance of the (1 1 0) and (2 0 0) diffraction peaks of sample Au/F-SBA-15-co (Fig. 1f) suggests that the one-pot synthesis method essentially afforded a highly ordered mesostructure of SBA-15. However, for catalyst Au/F-SBA-15-im (Fig. 1d) prepared using the impregnation method, the intensity of the (1 0 0) diffraction was dramatically decreased, implying partial structural collapses during the impregnation process.

Fig. 2 shows the N_2 adsorption/desorption isotherms and pore size distribution curves (inset) of samples. The textural properties are summarized in Table 1. All samples exhibited a typical type IV

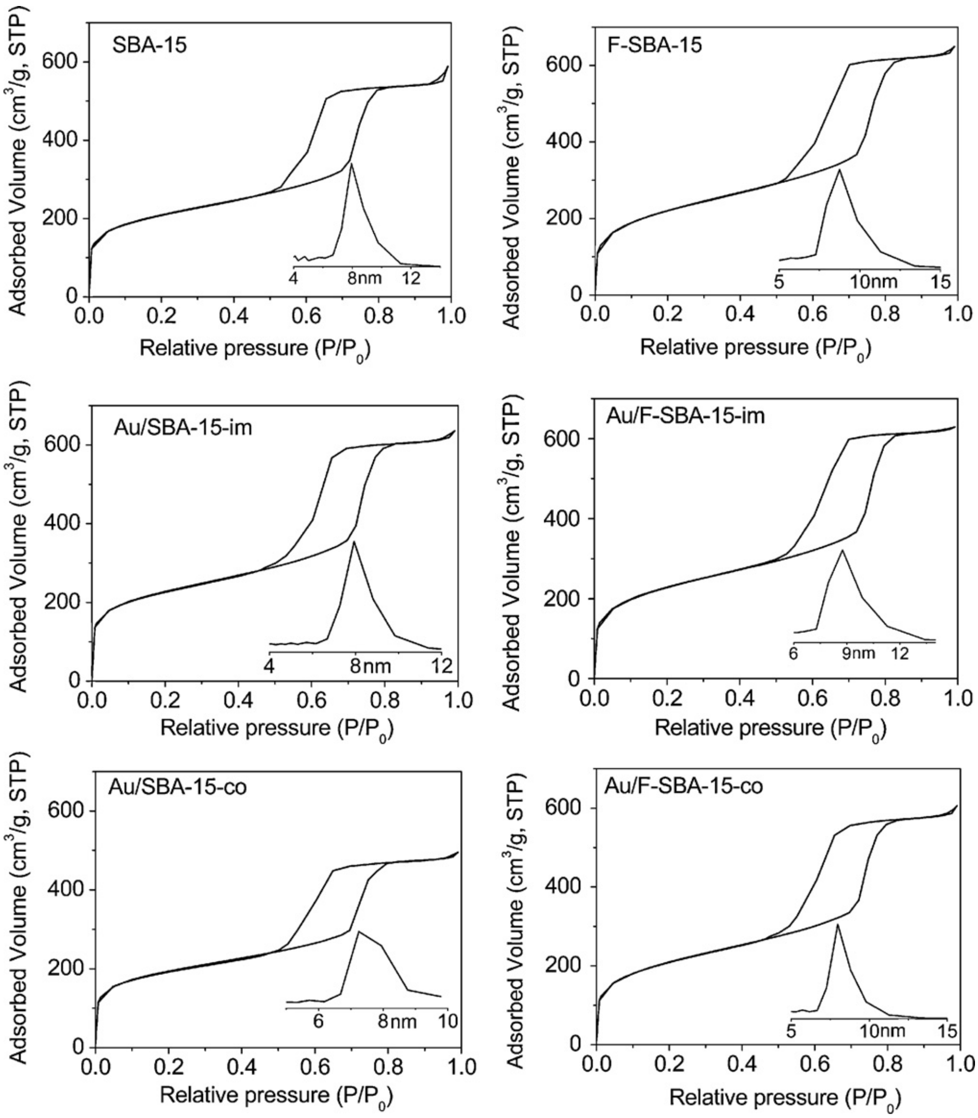

Fig. 2. N_2 adsorption/desorption isotherms and BJH pore size distribution curves (inset) of samples.

isotherm with a H-1 hysteresis loop [27], indicating all samples are mesoporous materials. The pore size distribution curves obtained with the BJH method are relatively narrow, showing the mesopores are ordered. From Table 1, it is seen that all vinyl-functionalized samples had higher specific surface area, larger pore size, and higher total pore volume than the non-functionalized ones. This is because minor framework condensation occurred in the hydrolysis process after introducing functional ligands, and the functionalized SBA-15 and its associated Au catalysts did not undergo the calcination process, thus less framework shrinkage and crystal wall crystallization occurred during the template removal step. Catalysts Au/SBA-15-co and Au/F-SBA-15-co derived from the one-pot synthesis method exhibited a thicker pore wall than that of the SBA-15 sample and the catalysts prepared using wet-impregnation method due to the salt effect of introducing Au precursor during the one-pot synthesis [28].

Table 1
Structural properties of supports and Au catalysts.

Materials	d_{100} (nm)	a (nm)	S_{BET} ($m^2\,g^{-1}$)	V ($cm^3\,g^{-1}$)	D_{ads} (nm)	t (nm)
SBA-15	8.7	10.0	782	1.0	7.9	2.1
Au/SBA-15-im	9.2	10.6	762	0.95	7.9	2.7
Au/SBA-15-co	8.9	10.3	645	0.76	7.3	3.0
F-SBA-15	8.9	10.3	796	1.0	8.7	1.6
Au/F-SBA-15-im	8.8	10.2	801	0.97	8.7	1.5
Au/F-SBA-15-co	9.2	10.6	785	0.93	8.0	2.6

Lattice parameter calculated from d_{100} spacing according to equation $a = 2d_{100}/\sqrt{3}$.
S_{BET}, surface area calculated using the BET method.
V, total pore volume calculated at $P/P_0 = 0.998$.
D_{ads}, pore diameter calculated using BJH method from the adsorption branch.
t, wall thickness obtained by subtracting pore diameter from lattice parameter.

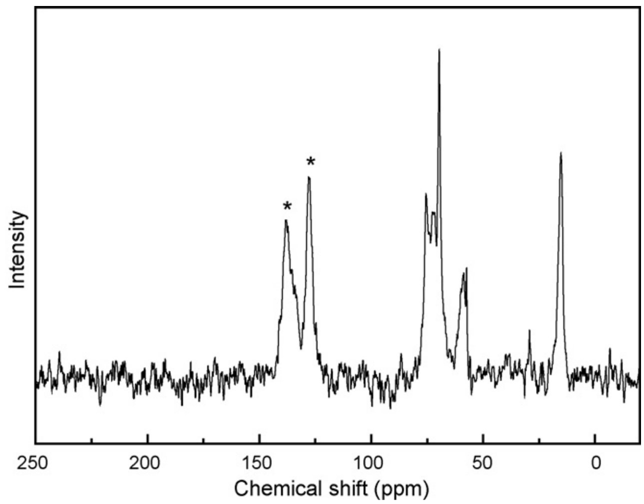

Fig. 3. ^1H–^{13}C CP/MAS NMR spectrum of catalyst Au/F-SBA-15-co.

The ^{13}C–^1H CP MAS NMR spectrum shown in Fig. 3 confirmed the presence of vinyl groups on sample Au/F-SBA-15-co because of the observation of two resonance peaks with chemical shifts of 129 and 135 ppm, which are due to vinyl groups [29]. The presence of surface vinyl groups can enhance the surface hydrophobicity of catalyst Au/F-SBA-15-co.

Fig. 4 shows the wide-angle XRD patterns of all Au catalysts prepared in this work. For samples Au/SBA-15-im (Fig. 4d), Au/F-SBA-15-im (Fig. 4c) and Au/F-SBA-15-co (Fig. 4a), two peaks at 38.18° and 44.43° two theta are seen. These are the characteristic peaks of the (1 1 1) and (2 0 0) reflections of cubic Au nanoparticles (JCPDS card no.: 4-784). The (2 2 0) peak at 64.55° two theta can also be seen on catalyst Au/F-SBA-15-im. For sample Au/F-SBA-15-co, the typical peaks due to cubic Au at 38.18° and 44.43° two theta are very weak. This is probably due to very small Au particle and/or a low loading of Au on the catalyst. No peak was observed from sample Au/SBA-15-co (Fig. 4b), showing the absence of Au nanoparticles or the particles were too small to be detected. This indicates that it is rather impossible to form Au nanoparticles on the surface of non-functionalized SBA-15 silica during the one-pot synthesis process.

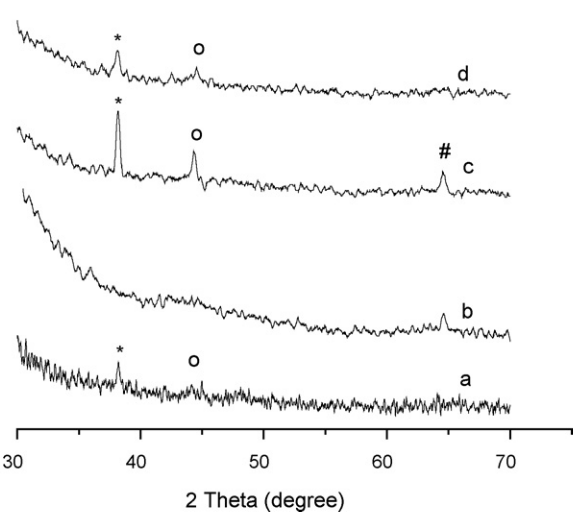

Fig. 4. Wide-angle XRD patterns of (a) Au/F-SBA-15-co; (b) Au/SBA-15-co; (c) Au/F-SBA-15-im, and (d) Au/SBA-15-im. *,° and # indicate the (1 1 1), (2 0 0) and (2 2 0) peaks of cubic Au, respectively.

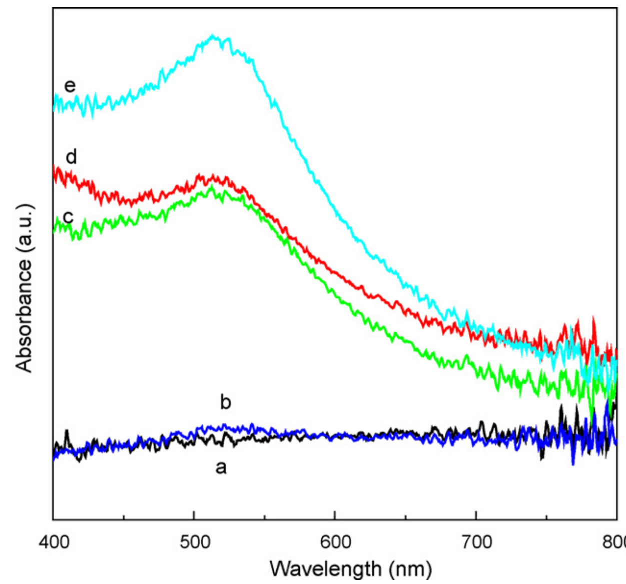

Fig. 5. UV–vis spectra of (a) F-SBA-15; (b) Au/SBA-15-co; (c) Au/F-SBA-15-im; (d) Au/SBA-15-im; (e) Au/F-SBA-15-co.

Au nanoparticles display a characteristic absorption band in the visible region due to Au surface plasma resonance (SPR) [30]. Fig. 5 shows the UV–vis spectra of samples F-SBA-15, Au/SBA-15-co, Au/SBA-15-im, Au/F-SBA-15-co, and Au/F-SBA-15-im. Sample F-SBA-15 (Fig. 5a) exhibited a featureless spectrum because of the absence of gold. A broad plasma resonance peak centered at about 518 nm can be seen on catalysts Au/F-SBA-15-im, Au/SBA-15-im and Au/F-SBA-15-co, indicating the existence of nano-sized Au particles [31]. It was reported that with the increase of Au particle size or aggregate size, the SPR peak shifts to longer wavelength or intensified at longer wavelength, that is, the original peak became broader and broader due to the coupling of the individual surface plasmon of nanoparticles in the aggregated structures caused by the self-assembly of Au NPs [32]. Thus, a sharper SPR peak of catalyst Au/F-SBA-15-co indicates a smaller Au particle size than that of catalysts Au/SBA-15-im and Au/F-SBA-15-im with dispersive SPR peaks. The plasma resonance peak cannot be seen on sample Au/SBA-15-co, indicating the absence of Au nanoparticles on this catalyst, consistent with the XRD results.

Fig. 6 shows the Au 4f XPS spectra of the catalysts. The Au 4f signal can be clearly seen from samples Au/SBA-15-im (Fig. 6a), Au/F-SBA-15-im (Fig. 6b) and Au/F-SBA-15-co (Fig. 6c), the presence of two peaks at binding energies of about 84.0 and 88.0 eV are assigned to metallic Au. The Au 4f signals cannot be found on sample Au/SBA-15-co (data not show here). In addition, compared to catalyst Au/SBA-15-im, the binding energy of Au 4f for catalysts Au/F-SBA-15-im and Au/F-SBA-15-co was shifted to low binding energy region, probably due to the interaction between Au nanoparticles and the catalysts support [33]. Fig. 6d shows the Au 4f XPS spectrum of catalyst Au/F-SBA-15-co before H_2 reduction. The Au $4f_{7/2}$ and $4f_{5/2}$ doublet with binding energy of 86.0 and 89.7 eV, respectively, corresponding to Au (III) complexes (86.2–87.0 and 89.0–90 eV) [34] indicated the presence of Au (III) complexes on catalyst Au/F-SBA-15-co before H_2 reduction. It can be concluded that after hydrothermal treatment, washing and surfactant extraction process, Au species were still firmly attached on the silica framework as Au (III) complex. Upon H_2 reduction, the Au (III) complexes were reduced to metallic Au^0.

Fig. 7 shows the TEM images of the Au catalysts. The average diameters of Au particles on catalysts Au/SBA-15-im (see Fig. 7a) and Au/F-SBA-15-im (see Fig. 7b) were estimated to be

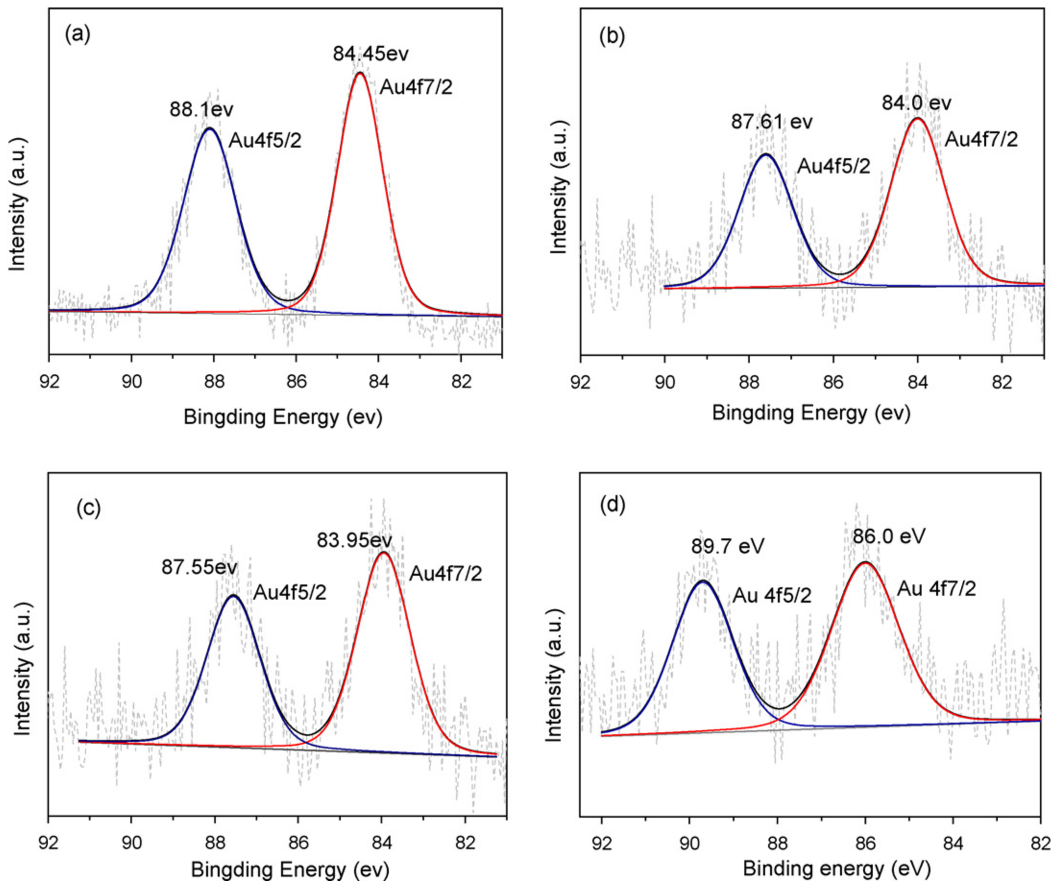

Fig. 6. Au 4f core-level XPS spectra of catalysts (a) Au/SBA-15-im; (b) Au/F-SBA-15-im; (c) Au/F-SBA-15-co; and (d) Au/F-SBA-15-co before H_2 reduction.

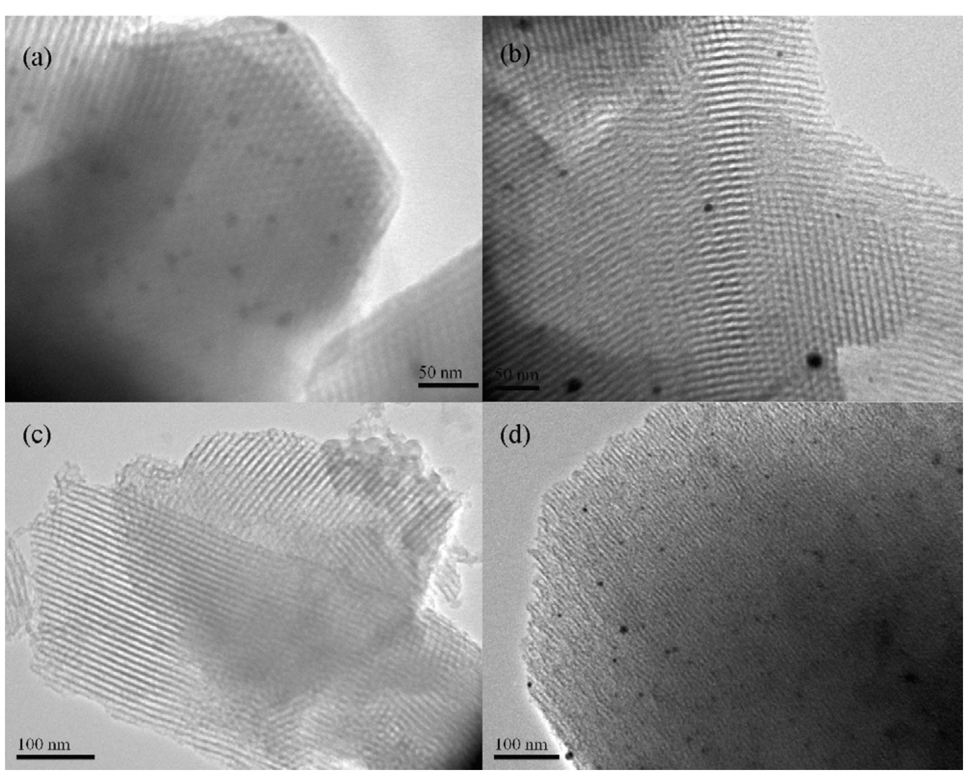

Fig. 7. TEM images of (a) Au/SBA-15-im; (b) Au/F-SBA-15-im; (c) Au/SBA-15-co; (d) Au/F-SBA-15-co.

about 8 and 9 nm, respectively. The bigger Au particle size on catalyst Au/F-SBA-15-im is mainly because the increase of surface hydrophobicity of F-SBA-15 support after introducing vinyl groups [35], which prohibited the diffusion of Au precursor solution into the pores of mesoporous silica during the wet-impregnation process, leading to the aggregation of gold particles on the external surface of functional support. The average diameter of Au particle on catalyst Au/F-SBA-15-co (see Fig. 7d) was estimated to be ∼5 nm, much smaller than that of catalysts prepared by wet-impregnation method, consistent with the UV–vis results. The smaller Au nanoparticle size on catalyst Au/F-SBA-15-co is due to the anchoring function of vinyl groups to Au precursors and Au nanoparticles, which led to the evenly dispersion of Au in the mesoporous silica support; at the same time, the template removing method is also very important to the Au particle size. In this work, the template P123 was removed by ethanol extraction instead of high temperature calcination, preventing the agglomeration of gold nanoparticles during heat treatment. The TEM image shown in Fig. 7c confirmed the absence of Au particles on catalyst Au/SBA-15-co. These results show that the organosilane, VTES, is a good functionality for anchoring Au nanoparticle during the one-pot synthesis process.

The XRD, UV–vis, XPS and TEM results discussed above showed that Au nanoparticles were present on catalysts Au/SBA-15-im, Au/F-SBA-15-im and Au/F-SBA-15-co as metallic Au. No Au nanoparticles were found on sample Au/SBA-15-co, due to the leaching of gold species during the washing step. This leaching did not occur over functionalized catalyst Au/F-SBA-15-co because the vinyl groups enhanced the interactions between the Au nanoparticles and the support. Such enhancement has been observed between Au nanoclusters and the π electrons of benzene rings [36,37]. The π electrons of vinyl groups in catalyst Au/F-SBA-15-co may similarly interact with Au nanoparticles in the present case.

The one-pot synthesis method for Au nanoparticles supported on vinyl-functionalized mesoporous silica materials is illustrated in Scheme 1. Complexation of vinyl groups with the gold ions offers a good opportunity for dispersion of $AuCl_4^-$ ions (Step 1). Condensation of TEOS with VTES in the presence of P123 micelles forms a mesophase with Au (III) complex wrapped in the organic region (supported by XPS results). Removal of the block copolymer template by ethanol leaves behind a mesoporous structure with Au ions complexes dispersed on the pore surface (Step 2). Finally, reduction of Au species to metallic Au nanoparticles by H_2 forms Au nanoparticles (Step 3). The distribution of Au nanoparticle size is controlled by the space confinement of silica matrix and the interaction of functional groups with Au nanoparticles. In this work, the space confinement was limited by the strong acid synthesis environment which is difficult for the attachment of gold nanoparticles in silica matrix, supported by the absence of Au nanoparticles on catalyst Au/SBA-15-co. Thus, the interaction of the functional groups with Au nanoparticles played the main role. A carbon–carbon double bond consists of one sigma bond and one π bond and the π electrons

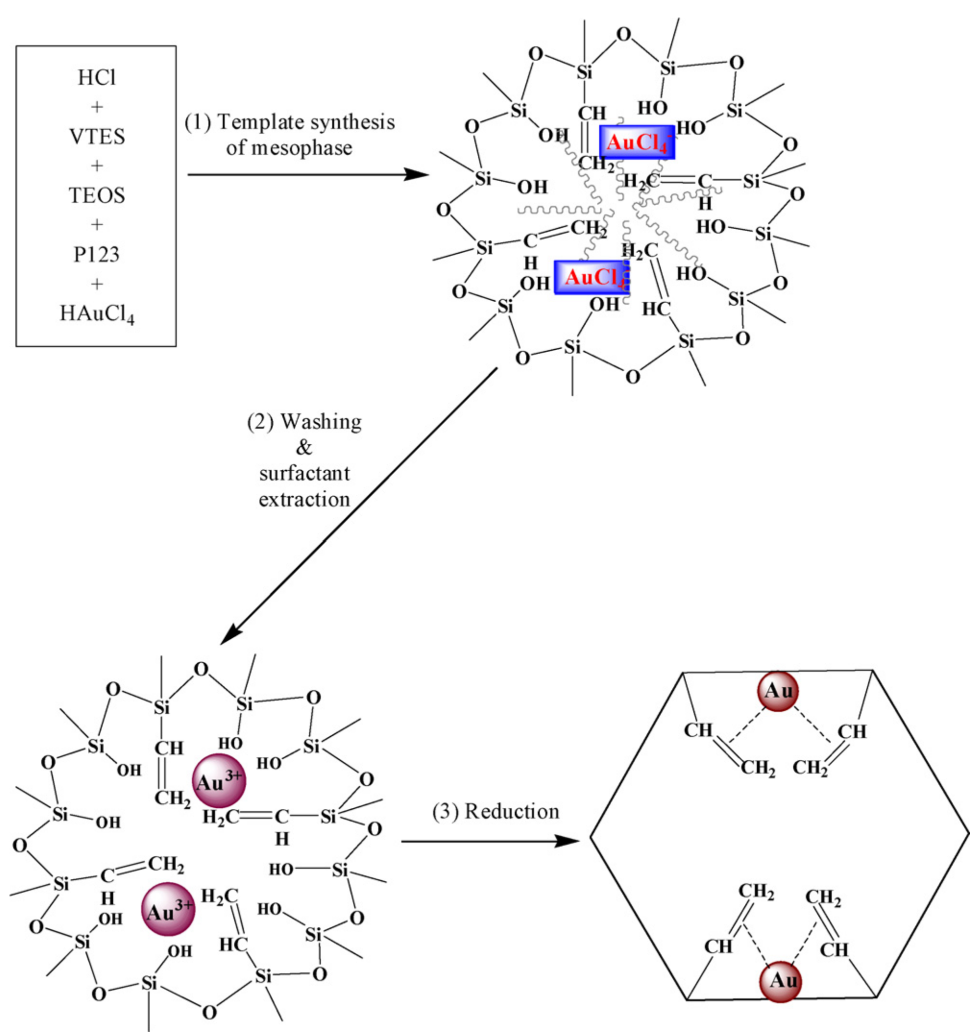

Scheme 1. Illustration of the one-pot method for the synthesis of Au nanoparticles supported on functionalized SBA-15.

Table 2
Catalytic properties in selective oxidation of cyclohexane.

Catalyst	Cyclohexane conversion (%)	K/A oil selectivity (%)[a]	Byproducts selectivity (%)
No catalyst	n.d.	n.d.	n.d.
SBA-15	n.d.	n.d.	n.d.
F-SBA-15	n.d.	n.d.	n.d.
Au/SBA-15-im	8.7	80.3	19.7
Au/F-SBA-15-im	8.4	79.2	20.6
Au/SBA-15-co	n.d.	n.d.	n.d.
Au/F-SBA-15-co	16.6	92.4	7.6

[a] Useful products include cyclohexanone and cyclohexanol; n.d.: not detectable.

are very active. On the other hand, a small number of holes formed in the *d*-band of Au caused by *d-s* hybridization [38]. The interaction between active π electrons of vinyl groups and the electron holes in the *d*-band of Au may have occurred during the synthesis of Au/F-SBA-15-co catalyst, leading to the good attachment and uniform dispersion of gold nanoparticles.

3.2. Selective oxidation of cyclohexane by molecular oxygen

The catalytic performance of the Au catalysts was evaluated in the selective oxidation of cyclohexane with molecular oxygen and reaction results are summarized in Table 2. It has been found that under the same reaction conditions, no conversion was observed in the absence of gold, i.e. using SBA-15 or functionalized SBA-15 (F-SBA-15) or in the absence of catalyst but with all other reaction components present, confirming that the catalysis is intimately involved with Au. Catalysts Au/SBA-15-im and Au/F-SBA-15-im exhibited almost the same activity and selectivity with a conversion of about 8% after 2 h of reaction. Catalyst Au/F-SBA-15-co exhibited the highest cyclohexane conversion of about 16.6%, doubling that of the catalysts prepared using the wet-impregnation method. It is interesting to note that the selectivity of cyclohexanone and cyclohexanol over catalyst Au/F-SBA-15-co was as high as 92.4%, higher than that over the catalysts prepared using the impregnation method. Au/SBA-15-co exhibited no activity due to the absence of Au nanoparticles.

After correlating the catalytic performance with the catalyst structure properties, it can be found that Au nanoparticles (Au^0) are the active sites for the cyclohexane oxidation and the particle size played an important role in the catalytic performance. Catalyst Au/F-SBA-15-co with an average Au particle size of about 5 nm showed a higher activity than catalysts Au/SBA-15-im and Au/F-SBA-15-im with average Au nanoparticle sizes of ~8 and ~9 nm, respectively. This was expected as smaller Au particles have a higher density of active surface Au atoms, which are favorable for the adsorption and activation of oxygen molecules during the oxidation reaction, leading to a higher catalytic activity.

Organic ligands play an important role in stabilizing Au nanoparticles on silica supports [39,40]. The influence of such functional groups on the catalytic reaction shall not be ignored. The observed good catalytic properties of catalyst Au/F-SBA-15-co is believed to be not only related to the Au particle size, but also the surface properties of the support. As cyclohexane is a non-polar organic compound, the increased surface hydrophobicity due to vinyl functional groups is more favorable for cyclohexane than for cyclohexanol and cyclohexanone, which are polar compounds. As illustrated in Scheme 2, oxygen molecules were adsorbed and activated by Au nanoparticles while cyclohexane molecules preferred the hydrophobic silica surface (Step I). Reaction between the adsorbed cyclohexane and dissociated oxygen produced intermediate cyclohexyl hydroperoxide (CHHP), which decomposed to form cyclohexanol and cyclohexanone adsorbed on the catalyst (Step II). These oxidation products can be further oxidized to byproducts, such as succinic acid and adipic acid, if they do not get rid of the surface promptly. Cyclohexane is preferentially adsorbed over cyclohexanol and cyclohexanone by catalyst Au/F-SBA-15-co because of the surface hydrophobicity of the catalyst (Step III), thus reducing the probability of deep oxidation to byproducts and resulting high useful products selectivity.

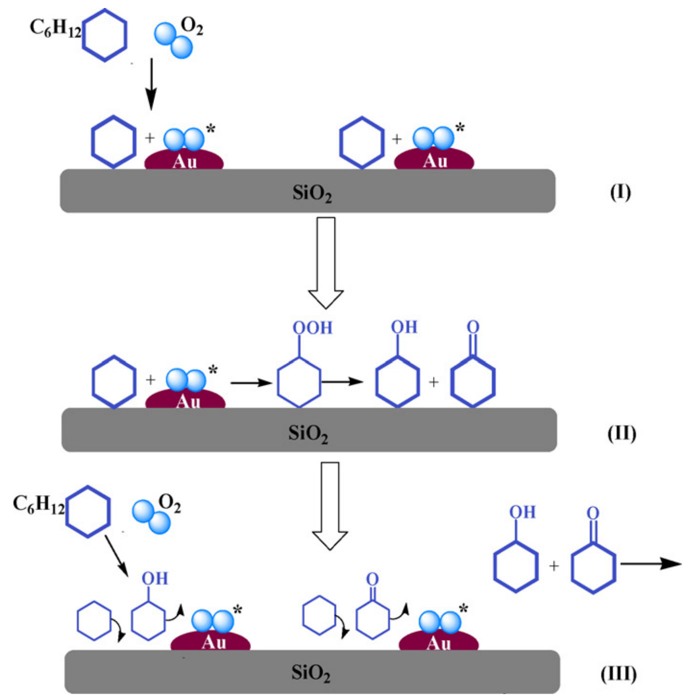

Scheme 2. Proposed mechanism of oxidation of cyclohexane on catalyst Au/F-SBA-15-co. (I) Adsorption and activation of oxygen and cyclohexane molecules; (II) oxidation of adsorbed cyclohexane to cyclohexanol and cyclohexanone; (III) competing adsorption and desorption of cyclohexane with cyclohexanol and cyclohexanone.

4. Conclusions

A one-pot synthesis method has been demonstrated to be a facile approach to prepare functionalized SBA-15 supported gold catalysts. Vinyl group was found to be a good functionality for anchoring Au nanoparticles because of the strong interaction between the Au species and vinyl groups. It was observed that the Au catalyst prepared using the present method exhibited higher catalytic activity and K/A oil selectivity than the catalysts prepared using the impregnation method. This can be attributed to the uniform dispersion of Au nanoparticles of about 5 nm in size on vinyl-functionalized mesoporous silica support together with the enhancement of surface hydrophobicity upon functionalization. A competing adsorption and desorption mechanism was used to explain the high K/A oil selectivity on the catalyst prepared using the present method.

Acknowledgements

Financial support from MOE Tier 1 Grant (R279000224112) is acknowledged. PW wishes to thank National University of Singapore Nanoscience and Nanotechnology (NUSNNI) for offering a scholarship.

References

[1] E.V. Spinace, H.O. Pastore, U. Schuchardt, J. Catal. 157 (1995) 631.
[2] M.H. Zahedi-Niaki, M.P. Kapoor, S. Kaliaguine, J. Catal. 177 (1998) 231.

[3] S.S. Lin, H.S. Weng, Appl. Catal. A 105 (1993) 289.
[4] R. Zhao, Y.Q. Wang, Y.L. Guo, Y. Guo, X.H. Liu, Z.G. Zhang, Y.S. Wang, W.C. Zhan, G.Z. Lu, Green Chem. 8 (2006) 459.
[5] B. Moden, B.Z. Zhan, J. Dakka, J.G. Santiesteban, E. Iglesia, J. Phys. Chem. C 111 (2007) 1402.
[6] S.E. Dapurkar, A. Sakthivel, P. Selvam, New J. Chem. 27 (2003) 1184.
[7] S. Samanta, N.K. Mal, A. Bhaumik, J. Mol. Catal. A 236 (2005) 7.
[8] H. Zhao, J.C. Zhou, H. Luo, C.Y. Zeng, D.H. Li, Y.J. Liu, Catal. Lett. 108 (2006) 49.
[9] N. Perkas, Y. Koltypin, O. Palchik, A. Gedanken, S. Chandrasekaran, Appl. Catal. A—Gen. 209 (2001) 125.
[10] V. Kesavan, D. Dhar, Y. Koltypin, N. Perkas, O. Palchik, A. Gedanken, S. Chandrasekaran, Proceedings of the 11th European Conference on Analytical Chemistry (EUROANALYSIS 11), Lisbon, Portugal, Sept. 03–08, 2000.
[11] J.M. Thomas, B.F.G. Johnson, R. Raja, G. Sankar, P.A. Midgley, Acc. Chem. Res. 36 (2003) 20.
[12] L.P. Zhou, J. Xu, H. Miao, F. Wang, X.Q. Li, Appl. Catal. A—Gen. 292 (2005) 223.
[13] M. Haruta, T. Kobayashi, H. Sano, N. Yamada, Chem. Lett. (1987) 405.
[14] M. Haruta, S. Tsubota, T. Kobayashi, H. Kageyama, M.J. Genet, B. Delmon, J. Catal. 144 (1993) 175.
[15] M. Haruta, Workshop on Environmental Catalysis—The Role of IB Metals, Ikeda, Japan, Nov. 02–03, 1995.
[16] L. Guczi, G. Peto, A. Beck, K. Frey, O. Geszti, G. Molnar, C. Daroczi, J. Am. Chem. Soc. 125 (2003) 4332.
[17] R. Zhao, D. Ji, G.M. Lv, G. Qian, L. Yan, X.L. Wang, J.S. Suo, Chem. Commun. (2004) 904.
[18] G.M. Lu, R. Zhao, G. Qian, Y.X. Qi, X.L. Wang, J.S. Suo, Catal. Lett. 97 (2004) 115.
[19] G.M. Lu, D. Ji, G. Qian, Y.X. Qi, X.L. Wang, J.S. Suo, Appl. Catal. A—Gen. 280 (2005) 175.
[20] L.X. Xu, C.H. He, M.Q. Zhu, S. Fang, Catal. Lett. 114 (2007) 202.
[21] L.X. Xu, C.H. He, M.Q. Zhu, K.J. Wu, Y.L. Lai, Catal. Commun. 9 (2008) 816.
[22] D.Y. Zhao, J.L. Feng, Q.S. Huo, N. Melosh, G.H. Fredrickson, B.F. Chmelka, G.D. Stucky, Science 279 (1998) 548.
[23] M.T. Bore, H.N. Pham, E.E. Switzer, T.L. Ward, A. Fukuoka, A.K. Datye, J. Phys. Chem. B 109 (2005) 2873.
[24] B. Lee, Z. Ma, Z.T. Zhang, C. Park, S. Dai, Micropor. Mesopor. Mater. 122 (2009) 160.
[25] M.T. Bore, H.N. Pham, T.L. Ward, A.K. Datye, Chem. Commun. (2004) 2620.
[26] K.K. Zhu, J.C. Hu, R. Richards, Catal. Lett. 100 (2005) 195.
[27] K.S.W.S.S.J. Gregg, Adsorption Surface Area and Porosity, Academic Press, London, 1995.
[28] B.L. Newalkar, S. Komarneni, Chem. Mater. 13 (2001) 4573.
[29] H.M. Kao, J.D. Wu, C.C. Cheng, A.S.T. Chiang, Micropor. Mesopor. Mater. 88 (2006) 319.
[30] S. Underwood, P. Mulvaney, Langmuir 10 (1994) 3427.
[31] S. Link, M.A. El-Sayed, J. Phys. Chem. B 103 (1999) 4212.
[32] K.H. Su, Q.H. Wei, X. Zhang, J.J. Mock, D.R. Smith, S. Schultz, Nano Lett. 3 (2003) 1087.
[33] Z. Zhong, J. Ho, J. Teo, S. Shen, A. Gedanken, Chem. Mater. 19 (2007) 4776.
[34] A. McNeillie, D.H. Brown, W.E. Smith, M. Gibson, L. Watson, J. Chem. Soc. -Dalton Trans. 5 (1980) 767.
[35] M.C. Burleigh, M.A. Markowitz, S. Jayasundera, M.S. Spector, C.W. Thomas, B.P. Gaber, J. Phys. Chem. B 107 (2003) 12628.
[36] T. Maddanimath, A. Kumar, J. D'Arcy-Gall, P.G. Ganesan, K. Vijayamohanan, G. Ramanath, Chem. Commun. (2005) 1435.
[37] G. Ramanath, J. D'Arcy-Gall, T. Maddanimath, A.V. Ellis, P.G. Ganesan, R. Goswami, A. Kumar, K. Vijayamohanan, Langmuir 20 (2004) 5583.
[38] C.L. Geoffrey, C. Bond, T. David, Tompson, Catalysis by Gold, Imperial College Press, London, 2006.
[39] L.F. Chen, J.C. Hu, R. Richards, J. Am. Chem. Soc. 131 (2009) 914.
[40] H.G. Zhu, B. Lee, S. Dai, S.H. Overbury, Langmuir 19 (2003) 3974.